ACS APPLIED MATERIALS & INTERFACES

Research Article

www.acsami.org

Electric Field-Controlled Ion Transport In TiO_2 Nanochannel

Dan Li, Wenheng Jing,* Shuaiqiang Li, Hao Shen, and Weihong Xing*

State Key Lab of Material-Oriented Chemical Engineering, National Engineering Research Center for Special Separation Membrane, College of Chemistry and Chemical Engineering, Nanjing Tech University, Nanjing, Jiang Su 210009, China

Supporting Information

ABSTRACT: On the basis of biological ion channels, we constructed TiO_2 membranes with rigid channels of 2.3 nm to mimic biomembranes with flexible channels; an external electric field was employed to regulate ion transport in the confined channels at a high ionic strength in the absence of electrical double layer overlap. Results show that transport rates for both Na^+ and Mg^{2+} were decreased irrespective of the direction of the electric field. Furthermore, a voltage-gated selective ion channel was formed, the Mg^{2+} channel closed at −2 V, and a reversed relative electric field gradient was at the same order of the concentration gradient, whereas the Na^+ with smaller Stokes radius and lower valence was less sensitive to the electric field and thus preferentially occupied and passed the channel. Thus, when an external electric field is applied, membranes with larger nanochannels have promising applications in selective separation of mixture salts at a high concentration.

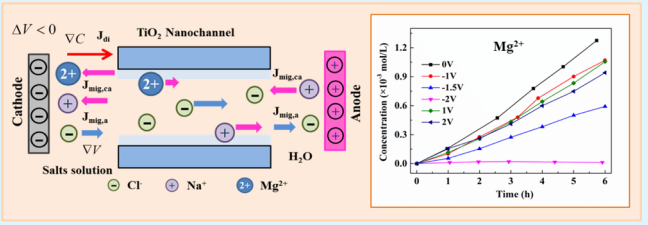

KEYWORDS: *ion transport, TiO_2 membrane, confined channel, electric field, TiO_2 nanochannel*

INTRODUCTION

Ion transport in a confined channel whose characteristic length scale is comparable to the range of several important forces including steric interactions (∼1−2 nm range), van der Waals force (∼1−50 nm) and electrostatic interactions (∼1−100 nm)[1] has attracted great attention owing to the emergence of novel transport phenomena and promising applications in desalination, molecule sensors, and energy conversion.[2−7] Among these forces, electrostatic interactions have been widely studied. In a nanochannel−solution interface, counterions accumulate near the charged surface, and the co-ions are repelled, creating an electrical double layer (EDL) region in which the potential decay with a characteristic length is known as the Debye length (λ).[8,9] Generally, the thickness of EDL decreased with the increase of ionic concentration.[10] For a channel with a size of 10 nm, to obtain a satisfactory EDL overlap, the ionic concentration should be smaller than 10 mM, which is far lower than the concentration of a realistic solution. Hence, for applications in practical physiological media, the size of confined channels should be reduced to a smaller size of ∼2 nm.

Inspired by ion and molecule transport in biological ion channels, the electrical manipulation of ions, proteins, and DNA in manufactured nanochannels have received enormous attention.[11−13] Using an applied external electric field, the surface charge property of a channel can be tuned, in turn controlling the transport of ion species.[14−16] Notably, different ions respond to the field effect differently. Mahurin et al. found that the transport of dye ions through a mesoporous carbon membrane could be prevented by an applied potential of −0.5 V, while the smaller K^+ and Na^+ required a larger applied potential.[17] Furthermore, the magnitude of a direct field effect control over the charged species in nanochannels is highly dependent on solution concentration.[18−20] It has been demonstrated that field-effect can more effectively control ion transport when the pore size is close to the thickness of the EDL in which the ion transport is governed by surface charge.[21−24] Hence, a confined channel with a size of ∼2 nm will have application in solutions with a wide range of ion concentrations. However, at such scales, the other forces (steric force and van der Waals) become very important apart from electrostatic interactions, making the ion transport behavior more complex. Some anomalous phenomena such as high water, proton, and ion mobility may occur.[4,25,26] To date, the transport mechanism has still not been fully explored in such a small confined space because of the difficulty in manufacturing artificial structures at this scale.[25−28] Recent developments in the synthesis of ceramic membrane have made it possible to construct a rigid nanochannel with a uniform pore size distribution of ∼2 nm, which makes the membrane a promising candidate for investigating the ion transport behavior.[27,29−31]

In ceramic nanochannels, electrostatic-based ionic selectivity is highly dependent on the surface charge and solution properties. The main influencing factors of ion permeation through the channel are steric, Donnan, and dielectric exclusion effects, among which the Donnan effect plays an important role in low electrolyte concentrations, whereas the dielectric exclusion effect is the dominant influencing factor in high electrolyte concentrations.[32−34] Herein, a TiO_2-based, three-dimensional (3D) nanofluidic transport membrane with a pore

Received: February 15, 2015
Accepted: May 11, 2015
Published: May 11, 2015

DOI: 10.1021/acsami.5b01505
ACS Appl. Mater. Interfaces 2015, 7, 11294−11300

size of 2.3 nm was prepared. An external electric field was employed to gate or control the ion transport in the confined channel with nonoverlapped EDL.

EXPERIMENTAL METHODS

Materials. Tetrabutyl titanate ($Ti(OC_4H_9)_4$), acetylacetone-(AcAc), hydrochloric acid (HCl), and 1-butanol (C_4H_9OH, 99%) were obtained by Shanghai Lingfeng Chemical Reagent Co., Ltd. Nitric acid (68%) was produced by Yangzhou Hubao Chemical Reagents Co. Triblock copolymer L64 ($(EO)_{13}(PO)_{30}(EO)_{13}$; molecular weight (2900 Da) was purchased from Sigma-Aldrich and used as received. TiO_2 nanoparticles with a particle size of ~5 nm (P5) were provided by Xuan Cheng Jing Rui New Materials Co., Ltd. Magnesium chloride ($MgCl_2$) and sodium chloride (NaCl) were obtained from Xi Long Chemical Co., Ltd.

Construction of Nanochannels. The TiO_2-based membrane consisted of a macroporous support and a separation layer. The TiO_2 thin film was fabricated by a nanoparticle-modified polymeric sol–gel process. A solution of L64 in C_4H_9OH was added in a mixture of $Ti(OC_4H_9)_4$ and AcAc. Then, another solution composed of C_4H_9OH, nitric acid, and deionized water was added dropwise to the above solution. The stirring was maintained for 4h at 25 °C to obtained a transparent sol. The molar ratio of $Ti(OC_4H_9)_4$/L64/AcAc/C_4H_9OH/HNO_3/H_2O was 1:0.03:1:80:0.1:3. Then, P5 with a concentration of 0.2 g/L was added to the prepared sol and dispersed by stirring for 2h and ultrasonication for 30 min at 250 W.

A disc-shaped α-Al_2O_3 membrane with a diameter of 28.5 mm, a thickness of 2 mm, and an average pore size of 100 nm was used as the macroporous support. The prepared sol was spin-coated on the substrate at 3000 rpm for 30 s. The coated films were dried and aged for 12 h at 60 °C in an oven and then calcined in air at 400 °C with a heating and cooling rate of 0.5 °C/min. All the procedures were repeated four times to obtain an anatase TiO_2 mesoporous membrane.

Ion Permeation Measurement. Ion transport was investigated using a laboratory-scale experimental setup, as shown in Figure 1. A TiO_2 membrane with a surface area 3.14 cm^2 was placed between the two graphite electrode slices and divided the module into dialysate (A) and diffusate (B) tank. The TiO_2 separation layer faced A tank, where filled with a mixed solution (0.4 M $MgCl_2$+0.8 M NaCl). B tank filled with 0.1L deionized water. A peristaltic pump with a running speed of 100 mL/min was used to pump the solutions. An electrochemical workshop (GAMRY Instruments Reference 3000) was connected to a Ti electrode to supply a constant potential difference ΔV over the membrane ($\Delta V = V_A - V_B$, where V_A and V_B are the electrode potentials at the A and B side, respectively. $\Delta V > 0$ is positive potential, while $\Delta V < 0$ is negative potential). The samples in the A and B tanks were used to analyze the concentration of Na^+ and Mg^{2+} at a certain time interval, respectively, and the permeation flux (J) was indicated from the slope of the ion concentration in the diffusate tank.

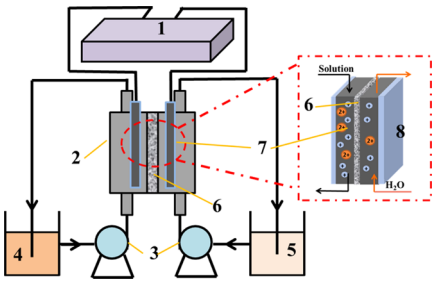

Figure 1. Schematic diagram of experimental setup: (1) DC power supply; (2) membrane module; (3) peristaltic pump; (4) dialysate tank; (5) diffusate tank; (6) TiO_2 membrane plate; (7) graphite electrode slice; and (8) Ti electrode.

Characterization. The mechanical property of the gel was analyzed by dynamic mechanical analysis in a compression mode and with an oscillating frequency of 1 Hz (DMA, Diamond DMA, PerkinElmer, Waltham, MA). The surface morphology and thickness of the membrane were observed by a field-emission scanning electron microscopy (FE-SEM, Hitachi S4800). The membrane permeability was determined by the permeation of deionized water at a transmembrane pressure of ~0.5 MPa. The separation capability of the membranes was evaluated by measuring 3g/L PEG solution with different molecular weights (10 000 Da, 6000 Da, 1500 Da, 600 Da) at a transmembrane pressure of ~0.5 MPa. The concentrations and molecular weights of PEG in the feed and permeate solutions were analyzed by gel permeation chromatography (Waters Co., Milford, MA). The concentrations of Na^+ and Mg^{2+} were analyzed by inductively coupled plasma atomic emission spectrometer (PerkinElmer Optima 7000DV). The impedance of the cell was analyzed using an electrochemical workstation in the range of 1 Hz to 1 MHz (GAMRY Instruments Reference 3000). The membrane and support were immersed in an electrolyte solution (0.4 M $MgCl_2$ +0.8 M NaCl) 12 h before testing to equilibrate the membrane. Additionally, the resistance of TiO_2 membrane and bare support were also analyzed, respectively, by directly covering them on the Ti electrode using Ag conductive adhesive.

RESULTS AND DISCUSSION

Construction of Titania 3D Nanochannels. The TiO_2 membrane was fabricated by a 5 nm TiO_2 nanoparticles-modified polymeric sol process using a disc-shaped α-Al_2O_3 membrane with an average pore size of 100 nm as support. After the P5 well-dispersed in the sol, the stiffness and ductility of the formed gel was investigated, and the results are shown in Figure 2. The TiO_2 gel with P5 nanoparticle exhibited an obvious enhancement of storage modulus (E′) and loss modulus (E″), indicating that the stiffness and ductility of the gel clearly improved. Accordingly, an integrated and crack-free membrane layer was more easily obtained, and the detail explanation was shown in our previous work.[35]

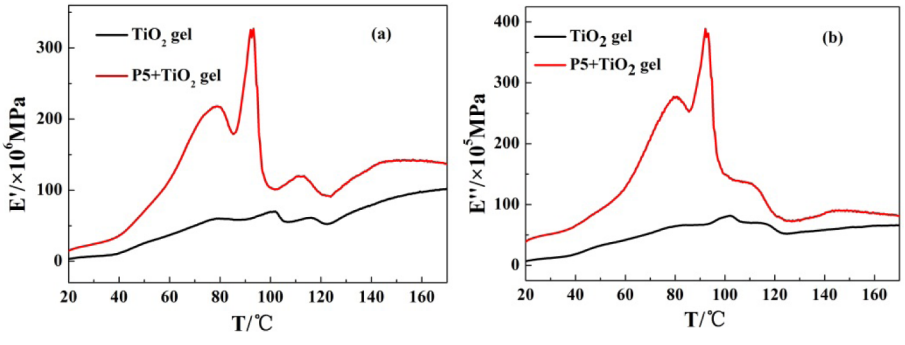

Figure 2. (a) Storage modulus–temperature curve of TiO_2 gel and (b) loss modulus–temperature curve of TiO_2 gel.

DOI: 10.1021/acsami.5b01505
ACS Appl. Mater. Interfaces 2015, 7, 11294–11300

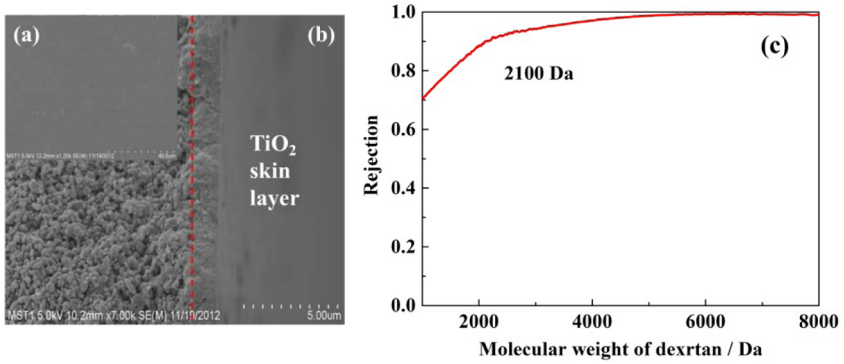

Figure 3. (a) FESEM images of the surface and (b) cross section of TiO_2 membrane; (c) PEG rejection curve of the resulting TiO_2 membrane.

After calcination, the resulting membrane presents an anatase phase (Supporting Information, Figure S1), and its surface morphology and cross-section are shown in Figure 3a,b. As observed from the images, the obtained TiO_2 membrane has an integrated and crack-free membrane layer with an approximate thickness of 1.5 μm. Through the pure water permeability and PEG retention experiments, the membrane showed a pure water flux of 2.2 $L{\cdot}m^{-2}{\cdot}h^{-1}{\cdot}bar^{-1}$and a 90% MWCO of 2100 Da (Figure 3c), equivalent to a molecular diameter of ~2.3 nm calculated using the formula, r (Å) = 0.262 × $(MW)^{1/2}$ − 0.3.[36] This indicates that 2.3 nm 3D nanochannels were successfully constructed by a 5 nm TiO_2 nanoparticle-modified sol−gel process, and rigid nanochannels are more advantageous and suitable for investigating ion transport.

Solution Resistance and Current Density. It is well-known that the ion conductance characteristic in a confined channel is highly dependent on the concentration. At low ionic concentration in the presence of EDL overlap, the conductance of the channel is governed by surface charge and the membrane behaves as a nonohmic resistor, while at high ionic concentration the conductance of the channel is governed by bulk ionic concentration and the membrane behaves as an ohmic resistor. In our experiment, the Debye length was estimated to be only ~0.21 nm using the equation $\kappa^{-1} = (\varepsilon_0\varepsilon_r k_B T/e^2\Sigma_i z_i^2 n_i^0)^{1/2}$, the electrical double layer only covered about 18% of the TiO_2 channel and 0.42% of substrate channel, respectively. In this case, the substrate and TiO_2 membrane mainly behaved as an ohmic resistor.

Figure 4 shows the Nyquist plots of the cell with and without membrane and support. As shown in Figure 4, the bulk electrolyte resistance between the two electrodes was ~11.84 Ω (x-intercept at the high-frequency region).[33] When the Ti electrode was covered by a bare substrate or supported TiO_2 membrane, no new capacitive loop emerged and only the ohmic resistance increased to 13.99 and 14.7 Ω, indicating that the resistance of the substrate alone and TiO_2 layer was 2.15 and 0.71 Ω, respectively. This increased resistance mainly originated from the geometric effects that the small porosity and tortured channel of the bare substrate and TiO_2 membrane increased the distance of the ion to arrive at the electrode. In addition, the slightly increased resistance of the TiO_2 layer indicated that the TiO_2 membrane revealed a relative small degree of blocking ion transfer at such a high electrolyte concentration.

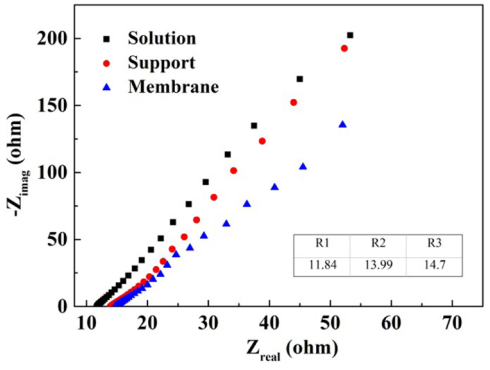

Figure 4. Nyquist plots of solution and membrane; (R1) solution resistance, (R2) solution + support resistance, and (R3) solution + membrane resistance.

Figure 5a shows the Nyquist plots of the cell at different times. At the beginning of the dialysis experiment, the diffusate tank was filled with the deionized water with weak conductivity. Therefore, the total solution resistance was relatively large in the initial stage of the experiment. As shown in Figure 5a, the total solution resistance of the cell after 20 min was 68.33 Ω. However, as the ions of the dialysate tank diffused through the membrane into the diffusate tank under a concentration gradient, the total solution conductance increased and the resistance decreased to 55.2 Ω after 40 min. Then, the decreasing trend became slower, and the resistance reached 33.71 Ω after 360 min. Figure 5b shows the current density curve at −2 V. The current density gradually increased as the ion passed through the membrane. Then the increasing trend decreased, and the cell showed a stable and high current density of ~1 mA/cm^2 after 360 min. At high concentration, the ion conductance was governed by bulk solution without EDL overlap, and thus, the high conductance resulted in a high current density.

Mixed Ions Transport Behavior in TiO_2 Nanochannel. As mentioned above, ion transport in nanochannels is strongly influenced by the interfacial charge property. Interestingly, the nanochannel constructed by TiO_2 material has an amphoteric surface, and its surface charge is determined by the solution environment. When the membrane surface comes into contact with the electrolyte solution, it can be negatively or positively charged by absorbing or releasing the ions. Hence, its surface charge properties highly depend on the concentration and pH of the background salt solution.[37,38] After the zeta potential (ξ) measurement, the isoelectric point of the synthesized TiO_2 material was ~3 (Supporting Information, Figure S2). As the pH of the mixed salts solution in the dialysate tank was ~5.27, the TiO_2 nanochannel surface was deprotonated and negatively charged, favoring the cation transport (Figure 6). When the

DOI: 10.1021/acsami.5b01505
ACS Appl. Mater. Interfaces 2015, 7, 11294−11300

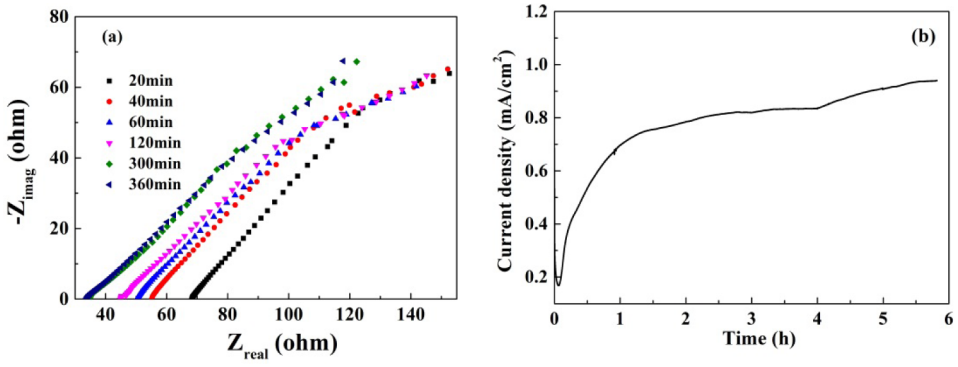

Figure 5. (a) Diagrams of Nyquist at different times. (b) Current density curve with time.

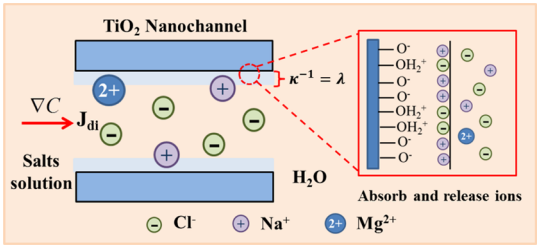

Figure 6. Schematic representation of ion transport behavior in the TiO_2 nanochannel. The nanochannel surface was negatively charged by absorption and releasing the ions. The ion flux (J_{di}) was developed by the concentration gradient (∇C).

ionic concentrations over the membrane were different, an ion flux (J_{di}) will be developed by the concentration gradient (∇C). In this study, there was a large concentration gradient and almost no EDL overlap in the membrane side, and thus, the ion will pass the membrane freely. As shown in Figure 7 and Table 1, the 3D TiO_2 channel showed a higher permeation flux of Na^+ than Mg^{2+} and relatively low Na^+/Mg^{2+} selectivity ($\alpha_{Na^+/Mg^{2+}}$) of 3.8, far smaller than that of nanofiltration membrane, 16, and only slightly higher than the ionic bulk diffusion coefficient ratio ($\alpha_{Na^+/Mg^{2+}} = J_{Na^+}/J_{Mg^{2+}} = 3.8$; bulk diffusion coefficient, $D_{Na^+} = 1.33 \times 10^{-9} m^2/s$; $D_{Mg^{2+}} = 0.72 \times 10^{-9}$ m^2/s; $D_{Na^+/Mg^{2+}} = 1.8$).[39]

It was generally accepted that nanofiltration membranes favored monovalent ion transport and rejected divalent or multivalent ions. This low $\alpha_{Na^+/Mg^{2+}}$ was attributed to the high ionic strength of the dialysate tank. The EDL only covered ~18% of the nanochannel, and the electrostatic effect was not very obvious. In addition, the Mg^{2+} solvation energy barrier was higher than that of Na^+ according to the dielectric exclusion effect, making it more difficult across the membrane (calculated by Zhao et al.[34] $\Delta W_{Na^+} = 1.88 \times 10^{-20} J$, $\Delta W_{Mg^{2+}} = 6.34 \times 10^{-20} J$). Therefore, because of the two effects, the $\alpha_{Na^+/Mg^{2+}}$ was slightly enhanced to the twice of the bulk diffusion coefficient ratio. This result agreed well with the low membrane resistance that 2.3 nm 3D TiO_2 confined channels showed a weak ability of blocking the ion transfer at high concentration.

In the presence of an electric field, an ion migration force is induced, driving the ions toward the oppositely charged electrode.[24,40] Taking a negative electric field for example, the induced electric field force will prevent the cation migration (Na^+ and Mg^{2+}, $J_{mig,ca}$) and facilitate the anion migration (Cl^-, $J_{mig,a}$) across the membrane, as shown in Figure 8. It had been demonstrated that the electric field effect highly depended on the ion size and valence.[17,41] The ion with a larger Stokes radius reveals a low mobility and is more easily captured by the electric field. In addition, the field effect is proportional to the ion valence. The ion with a higher valence is, the field effect is more remarkable. Because the Stokes radii of the Na^+ and Mg^{2+} are larger than that of Cl^- (Stokes radius: $r_{Na^+} = 0.184$ nm; $r_{Mg^{2+}} = 0.347$ nm; $r_{Cl^-} = 0.121$ nm) and Mg^{2+} possesses a higher valence, the magnitude electric migration flux of ions was $Mg^{2+} > Na^+ > Cl^-$. Hence, the net flux of cations decreased at a negative electric field, in which the direction of the applied electric field was opposite to the concentration gradient. When the applied electric field was strong enough, the induced flux was $|J_{mig}| > |J_{di}|$, resulting in hindering the ion transfer. To test this hypothesis, a negative electric field was applied over the TiO_2 confined channels. As expected, the rates of Na^+ and Mg^{2+} transport through the membrane decreased as a result of the competition of concentration gradient and potential gradient, as

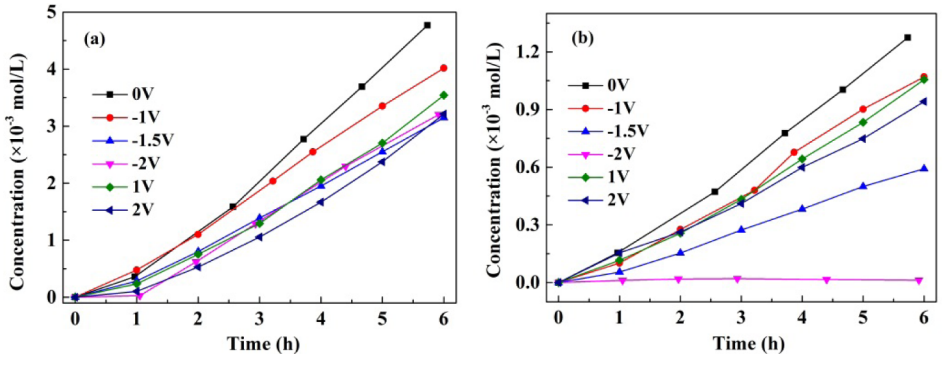

Figure 7. Ion concentrations in the diffusate tank at different applied voltages. (a) Na^+ and (b) Mg^{2+}.

DOI: 10.1021/acsami.5b01505
ACS Appl. Mater. Interfaces 2015, 7, 11294−11300

Table 1. Permeate Flux of Ions under Different Applied Potential

		potential (V)					
		0	−1	−1.5	−2	1	2
ion selectivity	$\alpha_{Na^+/Mg^{2+}}$	3.8	3.7	5.2	∼∞	3.3	3.5
flux (mol/(m^2·h))	Na^+	0.272	0.220	0.172	0.186	0.191	0.174
	Mg^{2+}	0.072	0.059	0.033	∼0	0.057	0.049

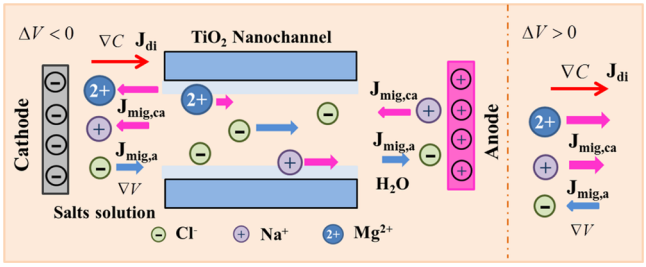

Figure 8. Schematic representation of the electric field influenced the ions transport behavior in the negative charged channel. In the presence of an applied potential, it induced an ion migration force to drive the ion toward the oppositely charged and developed a ion flux ($J_{mig,ca}$, $J_{mig,a}$).

shown in Figure 7 and Table 1. In particular, at −2 V, the perfectly separating the monovalent and divalent ions was achieved that the passage of the Mg^{2+} was completely prevented, whereas Na^+ still went through the membrane, decreasing the flux from 0.272 to 0.186 mol/(m^2·h). Similar phenomena were also observed experimentally in nanotube, nanochannel or 3D membrane.[17,22,24] Most of them controlled the ion transport behavior in the presence of EDL overlap by an external electric field. However, in this case, the 2.3 nm 3D TiO_2 membrane was capable of gating the transport of Mg^{2+} by a negative electric field with only 18% EDL overlap. This was attributed to the difference of field effect that Mg^{2+} was more sensitive than Na^+ response to the electric field. Hence, Na^+ more easily escaped from the influence of the electric field, preferentially went through the small-size channel and Mg^{2+} ions were rejected at −2 V. The results indicated that the field-effect can be extended beyond the thickness of EDL, which was recently numerically demonstrated in mesoporous nanochannels by Liu et al.[42]

To explore this further, the membrane potential and relative electric field gradient ($\nabla\psi$:$\nabla\psi = C_iZ_i\ (F/RT)(dV_m/dx_m)$) developed by external electric field were calculated according the membrane resistance of 2.86 Ω (the detail calculation process is provided in the Supporting Information). For application an external electric field, it has been demonstrated that the electric field can influence the membrane potential (V_m) and in turn regulate the ion transport behavior. As observed form Table 2, the field induced V_m increased with the increasing of electric field strength. When the $\nabla\psi$ became comparable to the concentration gradient at −2 V, a voltage-gated selective ion channel was formed. In this case, the Mg^{2+} channel closed, whereas the Na^+ still passed the channel because of large concentration gradient and less sensitive to the electric field. However, the potential driving force of Mg^{2+} was relatively smaller compared to the concentration driving force. The possible reason was that it was a complicated process when an external field was applied. The counterions accumulated near the interface of electrode, resulting in the deviation of bulk ionic concentration.[24] In particular, this phenomenon would be more serious when a porous graphite electrode was employed. As a result, the real ∇C would be relatively smaller. Hence, it is concluded that the gating-effect could occurr when $\nabla\psi$ is comparable to the concentration gradient.

On the basis of the analysis above, it was not difficult to find that the flux would be enhanced if the direction of electric field was the same as the direction of concentration gradient. However, interestingly, the flux of Na^+ and Mg^{2+} still decreased when a positive electric field was applied, as shown in Figure 7 and Table 1. The results were mainly attributed to the two effects. On the one hand, the graphite electrode absorbed part of ions, causing the ∇C slightly decreased. On the other hand, a lot of proton generated because of the phenomenon of water electrolyzed, when a potential closed to the theoretical voltage of water electrolysis (1.26 V) was applied. The generated proton preferentially occupied the nanochannel and hindered the transport of Na^+ and Mg^{2+}. Hence, with the two effects, the transport of Na^+ and Mg^{2+} was slightly inhibited.

For comparison, the ion transport behaviors in the bare support were also investigated (Supporting Information, Figure S4). The support showed high diffusion flux of Na^+ and Mg^{2+}, and the transport rates of Na^+ and Mg^{2+} only slightly decreased in the macropore channel of support after applying an electric field. This result indicated the electric effect was not obviously in the 100 nm pore of support at such high ionic concentration, and the gating-effect of Mg^{2+} was mainly attributed to the 2.3 nm TiO_2 membrane layer.

CONCLUSION

In summary, 3D TiO_2 channels with a pore size of 2.3 nm were successfully fabricated by a 5 nm TiO_2 nanoparticle-modified polymeric sol−gel route. Then, the ion transport in the

Table 2. Membrane Potential and Relative Electric Field Gradient ($\nabla\psi$) developed by an External Electric Field Calculated According the Membrane Resistance of 2.86 Ω

	potential (V)		
	−1	−1.5	−2
steady-state current (mA)	0.041	0.75	2.967
membrane potential (mV)	0.118	2.145	8.486
$\nabla\Psi = C_iZ_i\ (F/RT)(dV_m/dx_m)$(mol/m^4)	-1.88×10^4	-3.471×10^4	-1.352×10^5
$\nabla\ C_{Na^+} = (dc_{Na^+}/dx)$ (mol/m^4)		4.159×10^5	
$\nabla\ C_{Mg^{2+}} = (dc_{Mg^{2+}}/dx)$ (mol/m^4)		3.232×10^5	

DOI: 10.1021/acsami.5b01505
ACS Appl. Mater. Interfaces 2015, 7, 11294−11300

confined channel was controlled by an applied electric field at a high concentration in the absence of EDL overlap. The results show that 3D TiO_2 channels revealed a high permeate flux of Na^+ and Mg^{2+}, and low Na^+/Mg^{2+} selectivity under a large concentration gradient. When an electric field was applied, the transport rates for both Na^+ and Mg^{2+} decreased. In particular, the transport of Mg^{2+} can completely be prevented at −2 V, whereas the Na^+ ions still went through the membrane because of its small Stokes radius and low valence, making it less sensitive to the electric field. The theoretical calculation also performed and showed that the relative electric field gradient was comparable to the concentration gradient at −2 V and the transport of Mg^{2+} was hindered. These results indicate that the gating effect could be extended beyond the EDL overlap in a confined channel, and the membranes with larger nanochannels have promising applications in selective separation of mixed salts solution at a high concentration by applying an external electric field.

■ ASSOCIATED CONTENT

Supporting Information

Wide-angle X-ray diffraction (WAXRD) patterns of TiO_2 material at 400 °C; surface zeta potential of the TiO_2 membrane under different pH values of the solution; detail calculation process of electric field driving force; and ion transport behavior in the bare support. The Supporting Information is available free of charge on the ACS Publications website at DOI: 10.1021/acsami.5b01505.

■ AUTHOR INFORMATION

Corresponding Authors

*Tel: +86-25-8358 9136. Fax: +86-25-8317 2292. E-mail: jingwh@njtech.edu.cn.

*Tel: +86-25-8358 9136. Fax: +86-25-8317 2292. E-mail: xingwh@njtech.edu.cn.

Notes

The authors declare no competing financial interest.

■ ACKNOWLEDGMENTS

The Innovative Research Team Program by the Ministry of Education of China (No. IRT13070). National Natural Science Foundation of China (21176116, 21125629, and B060306).

■ REFERENCES

(1) Israelachvili, J. *Intermolecular and Surface Force*, 2nd ed.; Academic Press: London. 1992, 3.

(2) Cohen-Tanugi, D.; Grossman, J. C. Water Desalination across Nanoporous Graphene. *Nano Lett.* **2012**, *12*, 3602−3608.

(3) Fornasiero, F.; Bin In, J.; Kim, S.; Park, H. G.; Wang, Y.; Grigoropoulos, C. P.; Noy, A.; Bakajin, O. pH-Tunable Ion Selectivity in Carbon Nanotube Pores. *Langmuir* **2010**, *26*, 14848−14853.

(4) Joshi, R. K.; Carbone, P.; Wang, F. C.; Kravets, V. G.; Su, Y.; Grigorieva, I. V.; Wu, H. A.; Geim, A. K.; Nair, R. R. Precise and Ultrafast Molecular Sieving Through Graphene Oxide Membranes. *Science* **2014**, *343*, 752−754.

(5) O'Hern, S. C.; Boutilier, M. S. H.; Idrobo, J. C.; Song, Y.; Kong, J.; Laoui, T.; Atieh, M.; Karnik, R. Selective Ionic Transport through Tunable Subnanometer Pores in Single-Layer Graphene Membranes. *Nano Lett.* **2014**, *14*, 1234−1241.

(6) Pendergast, M. M.; Hoek, E. M. V. A Review of Water Treatment Membrane Nanotechnologies. *Energy Environ. Sci.* **2011**, *4*, 1946−1971.

(7) Van Gestel, T.; Vandecasteele, C.; Buekenhoudt, A.; Dotremont, C.; Luyten, J.; Leysen, R.; Van der Bruggen, B.; Maes, G. Salt Retention in Nanofiltration with Multilayer Ceramic TiO_2 Membranes. *J. Membr. Sci.* **2002**, *209*, 379−389.

(8) Bocquet, L.; Charlaix, E. Nanofluidics, from Bulk to Interfaces. *Chem. Soc. Rev.* **2010**, *39*, 1073−1095.

(9) Daiguji, H. Ion Transport in Nanofluidic Channels. *Chem. Soc. Rev.* **2010**, *39*, 901−911.

(10) Mulder, M. *Basic Principles of Membrane Technology*, 2nd ed.; Kluwer Academic Publishers: Dordrecht, The Netherlands, 1997, 8582−8582.

(11) Fan, R.; Huh, S.; Yan, R.; Arnold, J.; Yang, P. Gated Proton Transport in Aligned Mesoporous Silica Films. *Nat. Mater.* **2008**, *7*, 303−307.

(12) Schasfoort, R. B. M.; Schlautmann, S.; Hendrikse, L.; van den Berg, A. Field-Effect Flow Control for Microfabricated Fluidic Networks. *Science* **1999**, *286*, 942−945.

(13) Yeh, L. H.; Hughes, C.; Zeng, Z.; Qian, S. Tuning Ion Transport and Selectivity by a Salt Gradient in a Charged Nanopore. *Anal. Chem.* **2014**, *86*, 2681−2686.

(14) Guan, W. H.; Reed, M. A. Electric Field Modulation of the Membrane Potential in Solid-State Ion Channels. *Nano Lett.* **2012**, *12*, 6441−6447.

(15) Benson, L.; Yeh, L. H.; Chou, T. H.; Qian, S. Field Effect Regulation of Donnan Potential and Electrokinetic Flow in a Functionalized Soft Nanochannel. *Soft Matter* **2013**, *9*, 9767−9773.

(16) Hughes, C.; Yeh, L. H.; Qian, S. Field Effect Modulation of Surface Charge Property and Electroosmotic Flow in a Nanochannel: Stern Layer Effect. *J. Phys. Chem. C* **2013**, *117*, 9322−9331.

(17) Surwade, S. P.; Chai, S. H.; Choi, J. P.; Wang, X.; Lee, J. S.; Vlassiouk, I. V.; Mahurin, S. M.; Dai, S. Electrochemical Control of Ion Transport through a Mesoporous Carbon Membrane. *Langmuir* **2014**, *30*, 3606−3611.

(18) Hayes, M. A. Extension of External Voltage Control of Electroosmosis to High-pH Buffers. *Anal. Chem.* **1999**, *71*, 3793−3798.

(19) Kuo, T. C.; Sloan, L. A.; Sweedler, J. V.; Bohn, P. W. Manipulating Molecular Transport through Nanoporous Membranes by Control of Electrokinetic Flow: Effect of Surface Charge Density and Debye Length. *Langmuir* **2001**, *17*, 6298−6303.

(20) Yeh, L. H.; Xue, S.; Joo, S. W.; Qian, S.; Hsu, J. P. Field Effect Control of Surface Charge Property and Electroosmotic Flow in Nanofluidics. *J. Phys. Chem. C* **2012**, *116*, 4209−4216.

(21) Daiguji, H.; Hwang, J.; Takahashi, A.; Kataoka, S.; Endo, A. Ion Transport in Mesoporous Silica SBA-16 Thin Films with 3D Cubic Structures. *Langmuir* **2012**, *28*, 3671−3677.

(22) Guan, W. H.; Li, S. X.; Reed, M. A. Voltage Gated Ion and Molecule Transport in Engineered Nanochannels: Theory, Fabrication and Applications. *Nanotechnology* **2014**, *25*, 1−19.

(23) Nam, S. W.; Rooks, M. J.; Kim, K. B.; Rossnagel, S. M. Ionic Field Effect Transistors with Sub-10 nm Multiple Nanopores. *Nano Lett.* **2009**, *9*, 2044−2048.

(24) Schmuhl, R.; Keizer, K.; van den Berg, A.; ten Elshof, J. E.; Blank, D. H. A. Controlling the Transport of Cations through Permselective Mesoporous Alumina Layers by Manipulation of Electric Field and Ionic Strength. *J. Colloid Interface Sci.* **2004**, *273*, 331−338.

(25) Duan, C.; Majumdar, A. Anomalous Ion Transport in 2 nm Hydrophilic Nanochannels. *Nat. Nanotechnol.* **2010**, *5*, 848−852.

(26) Holt, J. K.; Park, H. G.; Wang, Y. M.; Stadermann, M.; Artyukhin, A. B.; Grigoropoulos, C. P.; Noy, A.; Bakajin, O. Fast Mass Transport through Sub-2-Nanometer Carbon Nanotubes. *Science* **2006**, *312*, 1034−1037.

(27) Boffa, V.; ten Elshof, J. E.; Blank, D. H. A. Preparation of Templated Mesoporous Silica Membranes on Macroporous Alpha−alumina Supports via Direct Coating of Thixotropic Polymeric Sols. *Micropor. Mesopor. Mater.* **2007**, *100*, 173−182.

(28) Liu, H.; He, J.; Tang, J.; Liu, H.; Pang, P.; Cao, D.; Krstic, P.; Joseph, S.; Lindsay, S.; Nuckolls, C. Translocation of Single−Stranded DNA Through Single-Walled Carbon Nanotubes. *Science* **2010**, *327*, 64−67.

DOI: 10.1021/acsami.5b01505
ACS Appl. Mater. Interfaces 2015, 7, 11294−11300

(29) Cao, X. P.; Li, D.; Jing, W. H.; Xing, W. H.; Fan, Y. Q. Synthesis of Visible-Light Responsive C, N, and Ce Co-doped TiO_2 Mesoporous Membranes via Weak Alkaline Sol−Gel Process. *J. Mater. Chem.* **2012**, *22*, 15309−15315.
(30) Qi, H.; Zhu, G. Z.; Li, L.; Xu, N. P. Fabrication of a Sol−Gel Derived Microporous Zirconia Membrane for Nanofiltration. *J. Sol−Gel Sci. Techn.* **2012**, *62*, 208−216.
(31) Van Gestel, T.; Kruidhof, H.; Blank, D. H. A.; Bouwmeester, H. J. M. ZrO_2 and TiO_2 membranes for nanofiltration and pervaporation—Part 1. Preparation and Characterization of a Corrosion-Resistant ZrO_2 Nanofiltration Membrane with a MWCO < 300. *J. Membr. Sci.* **2006**, *284*, 128−136.
(32) Oatley, D. L.; Llenas, L.; Aljohani, N. H. M.; Williams, P. M.; Martinez-Llado, X.; Rovira, M.; de Pablo, J. Investigation of the Dielectric Properties of Nanofiltration Membranes. *Desalination* **2013**, *315*, 100−106.
(33) Yoo, H. D.; Jang, J. H.; Ryu, J. H.; Park, Y.; Oh, S. M. Impedance Analysis of Porous Carbon Electrodes to Predict Rate Capability of Electric Double-Layer Capacitors. *J. Power Sources* **2014**, *267*, 411−420.
(34) Zhao, K.; Ni, G. Dielectric Analysis of Nanofiltration Membrane in Electrolyte Solutions: Influences of Permittivity of Wet Membrane and Volume Charge Density on Ion Permeability. *J. Electroanal. Chem.* **2011**, *661*, 226−238.
(35) Li, D.; Wang, H.; Jing, W. H.; Fan, Y. Q.; Xing, W. H. Fabrication of Mesoporous TiO_2 Membranes by a Nanoparticle-Modified Polymeric Sol Process. *J. Colloid Interface Sci.* **2014**, *433*, 43−48.
(36) Singh, S.; Khulbe, K. C.; Matsuura, T.; Ramamurthy, P. Membrane Characterization by Solute Transport and Atomic Force Microscopy. *J. Membr. Sci.* **1998**, *142*, 111−127.
(37) Labbez, C.; Fievet, P.; Szymczyk, A.; Vidonne, A.; Foissy, A.; Pagetti, J. Analysis of the Salt Retention of a Titania Membrane Using the "DSPM" Model: Effect of pH, Salt Concentration, and Nature. *J. Membr. Sci.* **2002**, *208*, 315−329.
(38) Xu, Y. Z.; Lebrun, R. E. Investigation of the Solute Separation by Charged Nanofiltration Membrane: Effect of pH, Ionic Strength, and Solute Type. *J. Membr. Sci.* **1999**, *158*, 93−104.
(39) Cheng, C.; Yaroshchuk, A.; Bruening, M. L. Fundamentals of Selective Ion Transport through Multilayer Polyelectrolyte Membranes. *Langmuir* **2013**, *29*, 1885−1892.
(40) Kemery, P. J.; Steehler, J. K.; Bohn, P. W. Electric Field Mediated Transport in Nanometer Diameter Channels. *Langmuir* **1998**, *14*, 2884−2889.
(41) Pennathur, S.; Santiago, J. G. Electrokinetic Transport in Nanochannels. 1. Theory. *Anal. Chem.* **2005**, *77*, 6772−6781.
(42) Liu, Y.; Huber, D. E.; Tabard-Cossa, V.; Dutton, R. W. Descreening of Field Effect in Electrically Gated Nanopores. *Appl. Phys. Lett.* **2010**, *97*, 143109.

DOI: 10.1021/acsami.5b01505
ACS Appl. Mater. Interfaces 2015, 7, 11294−11300